JOURNAL OF MATERIALS SCIENCE 19 (1984) 3201–3210

Flexural studies of carbon fibres

J. L. G. Da SILVA*, D. J. JOHNSON
Textile Physics Laboratory, University of Leeds, Leeds, UK

Fracture faces of several commercially available carbon fibres have been examined in the scanning electron microscope (SEM) after tensile and flexural failure. There are marked differences between the faces obtained after flexural failure and those produced after tensile failure, in the case of all the PAN-based fibres studied. In contrast, there is very little difference between the fracture faces for the two modes of failure in a mesophase-pitch-based fibre. The circular cross-section PAN-based fibres of all types are more flexible and less brittle than both a high modulus bilobal cross-section PAN-based fibre and the mesophase-pitch-based fibre. These fracture studies indicate that the Reynolds–Sharp failure mechanism operates in both tensile and flexural modes so that fibres containing sheet-like structures will be more brittle and inflexible than those containing more highly inter-linked random structures.

1. Introduction

Although considerable effort has been applied to improve our understanding of structural features and failure mechanisms which limit tensile strength in carbon fibres, much less attention has been paid to deformations which involve compression or combined compression and tension. When a fibre is stressed to failure by the closure of a knot or a loop, the reduction of tensile strength is a measure of brittleness; the size of the knot or loop at failure is a measure of flexibility. Values of these two physical properties should be of considerable interest to those concerned with the behaviour of both carbon fibres and carbon-fibre composites, particularly in terms of crack propagation in composites under flexural deformation.

It is now well known that tensile strength is gauge-length dependent for carbon fibres made from both polyacrylonitrile (PAN) [1] and mesophase-pitch [2] precursors, with an inverse relationship which is a consequence of internal and surface flaws [3, 4]. These flaws have been well characterized by electron microscope investigations of PAN-based [5–7] and pitch-based [8] carbon fibres. Statistical estimates of intrinsic tensile strength in mesophase-pitch-based carbon fibres, based on flaw distributions, have been evaluated for the critical load-transfer length of 0.1 to 0.3 mm in composites, giving rise to estimates such as 5.3 GPa [2], 3.8 GPa [8], and 3.5 GPa [9, 10]. Since carbon fibres with tensile strengths up to 4.3 GPa are now available commercially, the lower values must be treated with reservation.

It has been shown recently [7] that, even when flaws are present in a fibre, tensile strength is limited by other structural factors and that tensile failure is best considered in terms of the Reynolds–Sharp mechanism. This mechanism involves crack propagation after basal plane failure initiated by shear stress in large misoriented crystallites, and leads to a value for the maximum tensile strength of around 5.2 GPa in Type I PAN-based fibres. In order to obviate the effects of flaws, Thorne [11] showed that loop tests for a PAN-based fibre can give a value for the effective tensile strength at a gauge length as low as 0.1 mm, and thus predicted an intrinsic strength of 6 GPa in Type I fibres. It must be emphasized that this type of estimate is highly dependent on the somewhat uncertain evaluation of surface strain in a deformed fibre, and must again be treated with reservation.

The work reported here is concerned with measurements of flexibility, brittleness, and intrinsic tensile strength at low gauge length, in a number of currently available Type I (HM)

*Present address: Centro Tecnico Aerospacial, CTA-IPD-PMR, 12 200 Sao Jose dos Campos, Brazil.

0022–2461/84 $03.00 + .12

TABLE I Tensile properties of Type I, Type II, and Type A PAN-based carbon fibres, and mesophase-pitch-based carbon fibre (Thornel P). Manufacturers' data.

Manufacturer	Fibre	E (GPa)	σ (GPa)	d (μm)
	Type I			
Courtaulds	HM-S Grafil	340	2.10	7.0
Union Carbide	Thornel P (VSB-32-0)	380	1.90	10.0
Celanese	Celion GY-70	539	1.96	8.4*
	Type II			
Toho Beslon	Sta-grade Besfight	240	3.73	7.0
Union Carbide	Thornel 300	230	3.10	7.0
	Type A			
Courtaulds	XA-S Grafil	230	2.90	7.0

E Young's modulus, manufacturer's value.
σ Tensile strength, manufacturer's value.
d Fibre diameter, * average for bilobal fibre.
Thornel is the registered trademark of Union Carbide Limited.
Celion is the registered trademark of Celanese Corporation.
Grafil is the registered trademark of Courtaulds Limited.
Besfight is the registered trademark of Toho Beslon Company Limited.

and Type II (HS) carbon fibres. In addition, a scanning electron microscope (SEM) has been used to compare fracture faces produced after failure under flexural deformation, with fracture faces obtained after failure in tension. Some tests were attempted with loops prepared following the method described by Sinclair [12]; these were unsatisfactory and knots were used exclusively for all subsequent flexural studies.

2. Experimental details

A number of fibres currently available were obtained from various manufacturers; of these, three Type I (high modulus), two Type II (high strength), and one Type A fibre were chosen for detailed study; five are from PAN precursors, and one from a mesophase pitch. The code names, and manufacturers of these fibres, together with their respective values of Young's modulus, tensile strength, and diameter, as taken from published data sheets, are given in Table I.

The values of Young's modulus and tensile strength for ten fibres from the types chosen were checked by measurement on an Instron 1122 tensile tester using both 100 mm and 20 mm gauge lengths, a cross-head speed of 2 mm min^{-1}, and a full-scale deflection load of 10 g. This minimum calibration load was unsuitable for accurate knot-strength determination, so, for this purpose, tests were carried out using an extensometer built in the laboratory some years ago and modernized recently by adding a load cell designed both for this instrument and for tensile testing within the SEM. The extensometer has a minimum cross-head speed of 5 mm min^{-1}, but can utilize a full-scale deflection load as low as 0.5 g. A check on the efficiency of this instrument was made by repeating the tensile tests on the chosen fibres.

It is possible to prepare two types of knot, Type O and Type U [13] (see Fig. 1, where two knots of 400 μm diameter in Besfight fibres are illustrated for comparison). Note that the ellipticity of the Type U knot is more pronounced, because the bight, or loop, is tilted with respect to the bight of the Type O knot. Tests showed that knot strengths were not significantly different for the two types of knot, and all work was subsequently carried out with Type O knots, which were slightly easier to prepare.

Two sets of specimens were used for fracture-face examination: (i) straight fibres stressed to failure at 20 mm gauge length in the extensometer; and (ii) fibres in Type O knots stressed to failure under the same conditions. All fracture faces were obtained in glycerol, which effectively damps the relatively large energy released on failure, and prevents multiple failure points and loss of the appropriate end [7]. For tensile failure, only fibres failing near the centre of the gauge length were chosen; for flexural failure, close observation was necessary so that the mode of failure could be determined and appropriate specimens saved. After removal of glycerol by washing, the fracture ends were mounted on speci-

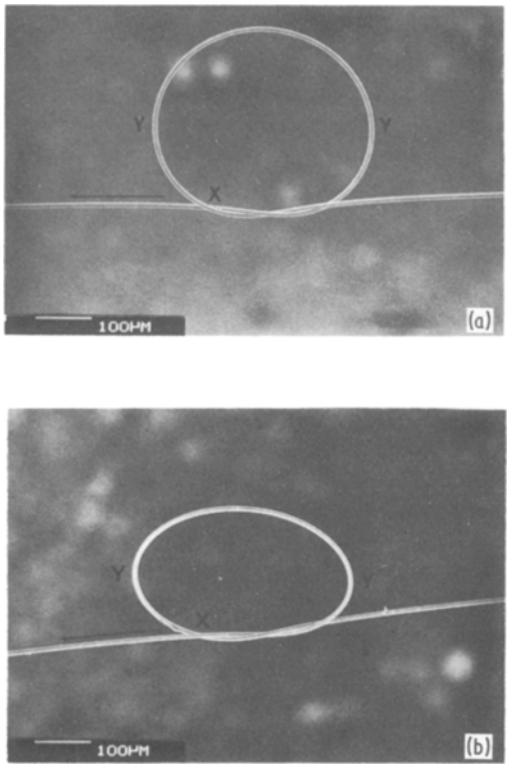

Figure 1 (a) Type O knot in Sta-grade Besfight. (b) Type U knot in Sta-grade Besfight.

men stubs and coated with gold by sputtering, prior to SEM examination.

For more detailed dynamic observation of flexural failure, and for measurement of the minimum radius of curvature of the knots, carbon fibres were stressed to failure within a Cambridge Stereoscan 150 Mk 2 electron microscope. In order to do this, a stage extensometer was used, which had been constructed for tensile testing on the stage of the SEM. The extensometer is shown in Fig. 2, where "m" marks a moveable arm, which is pulled away from the fixed arm "f" by means of a Kevlar "rope" "k" wound around a pulley turned by an Escap motor "E". The motor is driven at a selected speed by a pulsed power unit; movement of "m" is controlled precisely by means of a joy-stick. If necessary, the tension can be measured by means of strain gauges attached to arm "f"; this facility was not used in the work reported here.

Knots of type O (arrowed in Fig. 2) were fixed across the two arms, usually two at a time, and the stage extensometer placed in the SEM without gold coating of the fibres. In practice it was always possible to observe the closure of each knot individually as the arms were separated, because they were never of the same initial size. Each knot was pulled tight by small increments and micrographs were recorded as appropriate. At the same time, the major axis of the elliptical bright of the knot (YY′ in Fig. 1) was measured on the screen of the SEM. This measurement was always in agreement with that taken from the corresponding print. After some experience with each fibre specimen, the failure dimension of the knot could be predicted, thus fewer micrographs were taken at non-critical values. The actual failure value of YY′ is necessarily slightly lower than the last recorded value before failure.

3. Results

3.1. Brittleness and flexibility

The mean values of tensile strength σ and Young's modulus E at different gauge lengths as measured on the Instron, together with values measured on the extensometer at the shorter gauge length, are listed in Table II. Both modulus and strength are gauge-length dependent. It should be noted that the high standard deviation of the Celanese carbon fibre is a consequence of its bilobal cross-section and the wide variation in its effective radius. There is no significant difference between the tensile

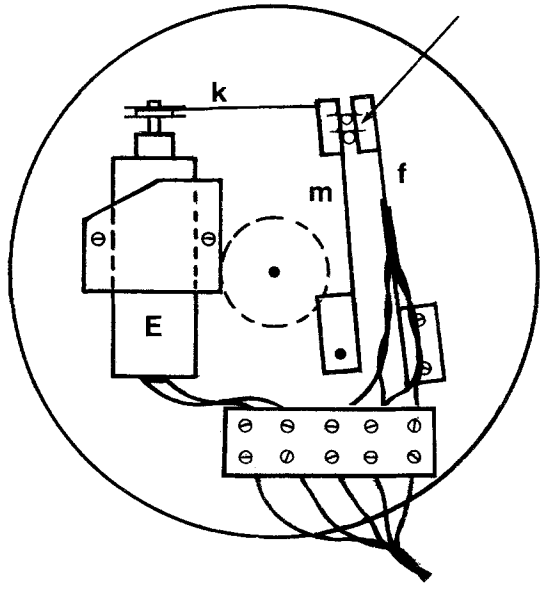

Figure 2 Stage extensometer for SEM, "E" ESCAP motor, "k" Kevlar rope, "m" moveable arm, "f" fixed arm.

TABLE II Tensile properties of Type I, Type II, and Type A PAN-based carbon fibres, and mesophase-pitch-based carbon fibre (Thornel P).

	Instron				Extensometer	
	100 mm gauge		20 mm gauge		20 mm gauge	
	E (GPa)	σ (GPa)	E (GPa)	σ (GPa)	E (GPa)	σ (GPa)
Type I						
HM-S Grafil	270	2.1	205	2.1	280	2.1
Thornel P (VSB-32-0)	400	1.3	260	1.6	260	1.6
Celion GY-70	500	1.5	350	1.8	340	1.8
Type II						
Sta-grade Besfight	240	2.8	215	3.8	220	3.6
Thornel 300	235	2.0	210	2.8	210	3.0
Type A						
XA-S Grafil	255	2.7	190	2.9	190	2.8

E Young's modulus.
σ Tensile strength.
Standard deviations are 0.4 to 0.6 for σ and 30 to 60 for E, except for Celion with SDs 0.7 for σ and 90 for E.

strength values obtained on the two instruments nor between these values and the manufacturers' quoted values. We are therefore confident that knot strengths have been measured accurately on the extensometer. These knot strengths are given in Table III together with the brittleness expressed as a ratio of tensile strength to knot strength.

Values for the flexibility of a fibre, expressed in terms of the major axis of the elliptical bight of the knot as measured from micrographs, are given in Table III. If we assume that the fibre fails when the elastic limit is exceeded, the surface tensile stress σ_s is given by

$$\sigma_s = Ed/D, \quad (1)$$

where E is the Young's modulus, d is the fibre diameter, and D the knot diameter at failure [11]. Use of Equation 1 assumed that the strain at the surface of a fibre in a knot is given by d/D. Twisting of the fibre may well reduce the strain at the surface; estimates of intrinsic tensile strength σ_i based on an arbitrary reduction of 50% are also given in Table III.

3.2. Tensile failure

Typical fracture faces for each of the six carbon fibres after tensile failure are illustrated in Figs. 3 to 8. There was little evidence of failure-initiating flaws in these surfaces but the PAN-based fibres show the typical striations radiating from the failure point after the glass-like region. The Besfight fibre, Fig. 3, has the most uniformly circular cross-section followed by both HM-S and XA-S Grafil, Figs. 4 and 5 respectively; in contrast, Thornel 300, Fig. 6, has a highly convoluted surface. The pitch-based carbon fibre, Fig. 7, is very circular and has a sheet-like structure which is also evident in cut faces. GY 70 is a bilobal fibre which has a very well-defined skin, Fig. 8. In all cases both fibre ends were examined after fracture. Fig. 6 shows the two complementary fracture faces in a Thornel 300 fibre after tensile failure.

3.3. Flexural failure

Visual observation of flexural failure, both in glycerol and in the SEM, showed two distinct modes of failure. All the high strength fibres –

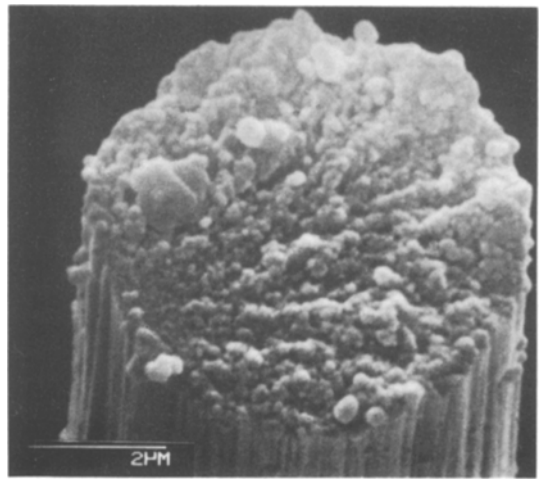

Figure 3 Fracture face of Sta-grade Besfight after tensile failure.

TABLE III Flexural properties of Type I, Type II and Type A PAN-based carbon fibres and mesophase-pitch-based carbon fibre (Thornel P).

	K (MPa)	σ/K (× 10)	YY′ (μm)	σ_i (GPa)
Type I				
HM-S Grafil	63	0.33	370	3.22
Thornel P (VSB-32-0)	10	1.90	840	2.26
Celion GY-70	6	3.27	980	*
Type II				
Sta-grade Besfight	93	0.40	230	3.65
Thornel 300	34	0.50	300	2.79
Type A				
XA-S Grafil	62	0.47	290	2.77

K Knot strength.
σ/K Brittleness.
YY′ Major axis of elliptical bight of knot before failure (Fig. 1).
σ_i Intrinsic tensile strength assuming surface tensile strain 50% d/D.
* Calculation invalid for bilobal cross-section fibre.

Besfight, XA-S Grafil and Thornel – break at or near the point marked X in Fig. 1, which is near the point of fibre cross-over closest to the end which is being pulled (arrowed). The high modulus fibres – HM-S Grafil, the pitch-based fibre and GY-70 – normally break simultaneously at the points YY′, where there is maximum curvature of the bight of the knot. HM-S Grafil is sometimes an exception, breaking at the point X. In glycerol it is possible to see one, two, or three pieces emerge after failure at YY′; in the SEM it is very rare to see separate pieces.

The fracture faces of the circular PAN-based carbon fibres after flexural failure are distinctly different from the faces after tensile failure. Fig. 9 shows the Besfight fibre, Fig. 10 complementary faces of the XA-S fibre, and Fig. 11 the Thornel 300 fibre, in each case after flexural failure in glycerol. These faces, all from Type II fibres, show a rough striated area and a relatively smooth area corresponding to the regions of the fibre under tension and compression, respectively. The Type I PAN-based fibre, HM-Grafil, has a much more deeply corrugated area between the smooth compression zone and the rough tension zone, Fig. 12. This probably corresponds to a region of the fibre under maximum shear stress.

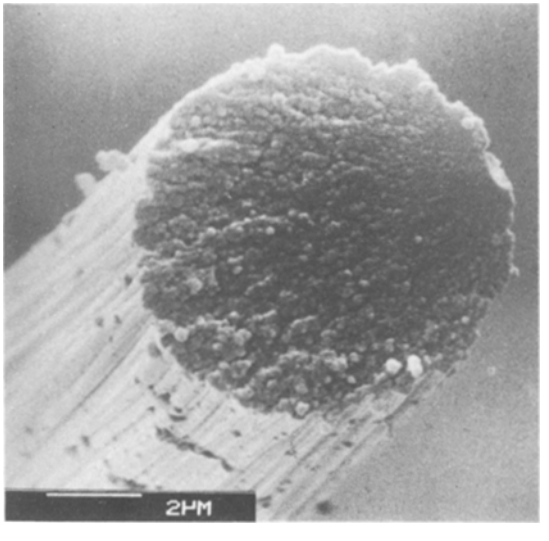

Figure 4 Fracture face of HM-S Grafil after tensile failure.

The fracture surface of the Thornel mesophase-pitch-based fibre is very similar in flexural failure (Fig. 13) to the surface produced by tensile failure, apart from a relatively small angled region (arrowed). The bilobal Celanese fibre has a very different fracture face in flexural failure (Fig. 14) from any other fibre, and is different from a typical fracture face after failure in tension. Part of the fibre has broken away at an angle to the cross-section, but there is no smooth area in this or the corresponding fracture face. Up to 15 separate pairs of fracture faces have been studied for each specimen; the faces represented here are typical and it is possible in some cases to identify the origin of the fibre by its fracture face after flexural failure.

4. Discussion

From the data presented in Table III, we may note that among the Type I fibres, the mesophase pitch-based Thornel P (VSB-32-0) and the PAN-based

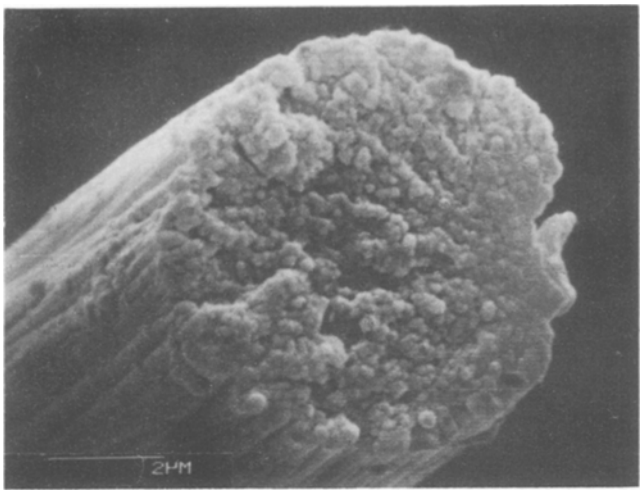

Figure 5 Fracture face of XA-S Grafil after tensile failure.

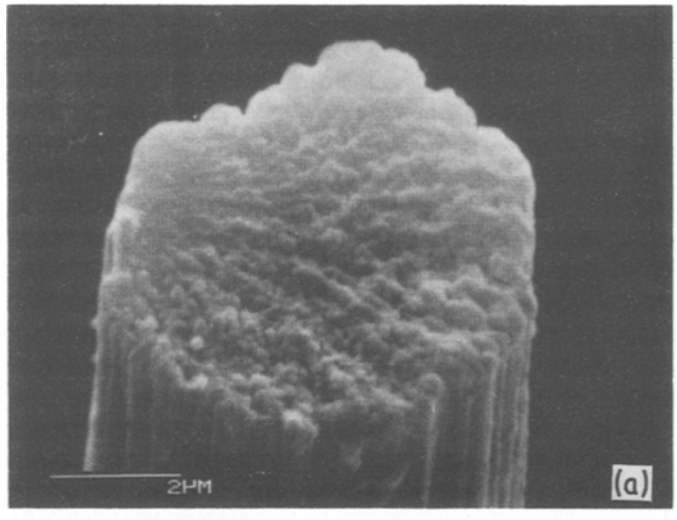

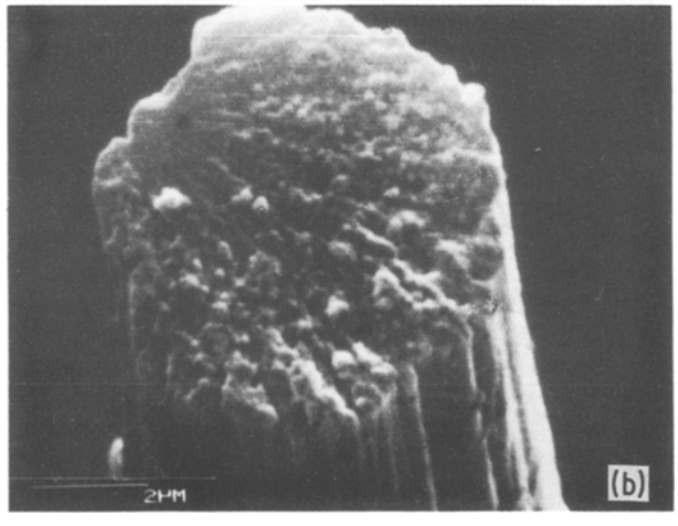

Figure 6 Complementary fracture faces of Thornel 300 after tensile failure.

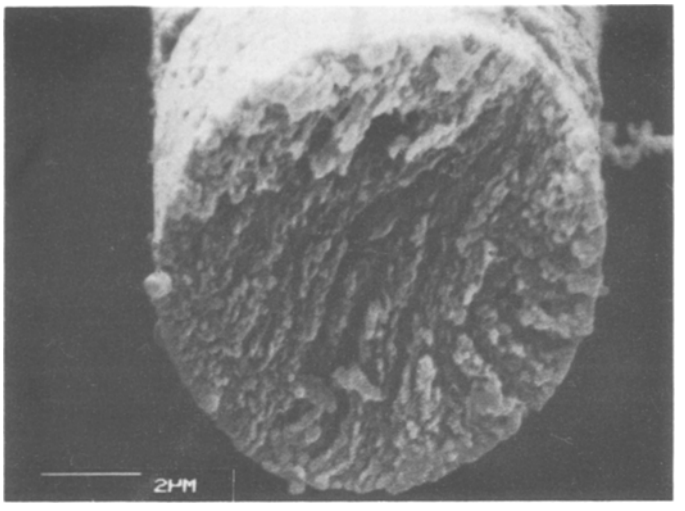

Figure 7 Fracture face of Thornel P after tensile failure.

Celion GY-70 are very much more brittle and inflexible than the PAN-based HM-S Grafil. Among the Type II and Type A fibres (all PAN-based), the Besfight fibre is least brittle and most flexible and has the highest tensile and knot strength. It is of interest that this fibre also has the most perfectly circular cross-section of all the fibres studied.

For most of the fibres there is very little difference between the intrinsic tensile strengths evaluated on the basis of an arbitrary surface strain of $d/2D$ and the manufacturers' quoted strengths, except for HM-S Grafil, which might be held to suggest the presence of a greater number of flaws in this fibre than in the others. However, careful examination of many micrographs, particularly from HM-S Grafil, reveals very little evidence for fracture initiating flaws in any of the fracture faces examined after tensile failure. This indicates that the population of gross defects in all of these fibres is low. Consequently the reason for the marked differences in brittleness and flexibility must be sought in the fine structure of the fibres.

Fracture faces from the Thornel pitch-based fibre, Fig. 7, show that there are sheet-like structures within the fibre. Although not as radial in structure as some of the earlier mesophase-pitch fibres, the most predominant macrostructural feature is sheet-like. These sheets can be expected to propagate a transverse crack, according to the Reynolds–Sharp fracture mechanism, much better than a random structure, because of the large effective crystallite size in that direction, which

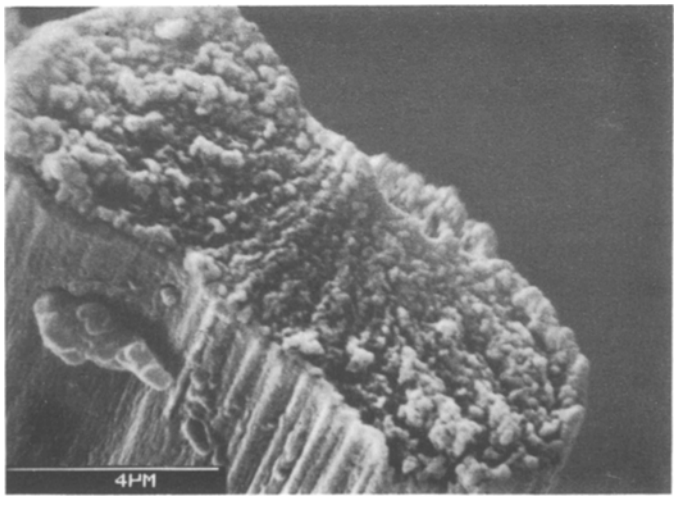

Figure 8 Fracture face of Celion GY-70 after tensile failure.

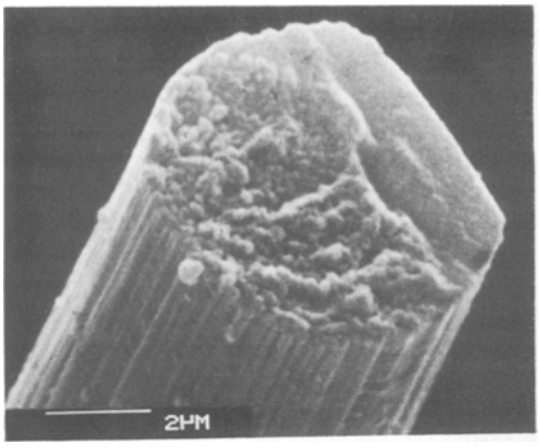

Figure 9 Fracture face of Sta-grade Besfight after flexural failure.

may well exceed the critical flaw size [7]. Misoriented crystallites are necessary to initiate failure; they can be observed in dark-field transmission electron microscope (TEM) images of these fibres, where, despite an overall improved orientation, they are not uncommon [14]. The uniformity of structure seen in a knot fracture face may indicate the simultaneous failure of sheets through that part of the section in tension. When the fibres are deformed into a knot, it is inevitable that many more crystallites are misoriented; consequently the changes of layer-plane rupture and subsequent fracture are increased.

Knot fracture faces from a GY-70 PAN-based fibre show both the bilobal shape and a very prominent sheath/core heterogeneity. There is no

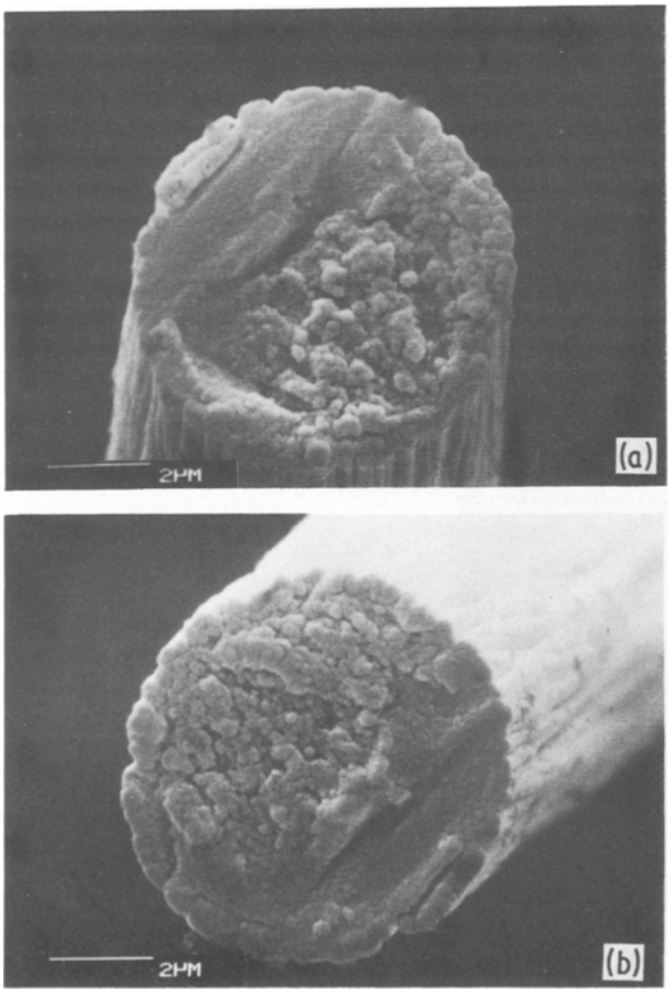

Figure 10 Complementary fracture faces of XA-S Grafil after flexural failure.

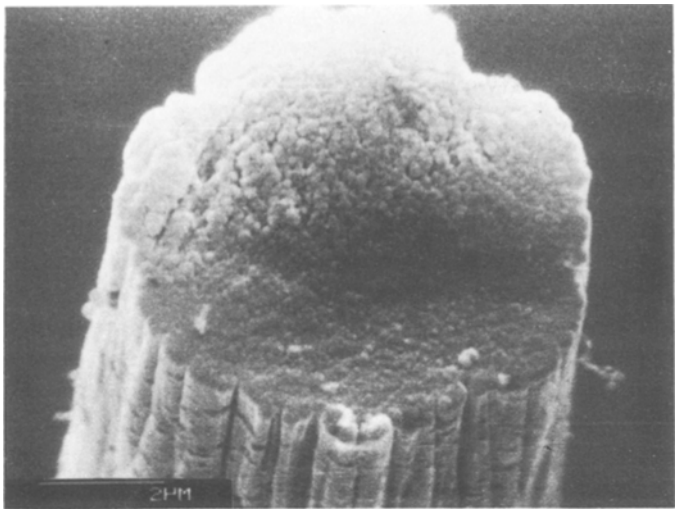

Figure 11 Fracture face of Thornel 300 after flexural failure.

evidence of sheet-like macrostructure. Indeed, the uniformity of the fracture face may again be indicative of the simultaneous failure of the structural elements which are misoriented by bending. Certainly this fibre has a relatively large crystallite size in terms of both Lc* (10 nm) and La* (17 nm), as measured by X-ray diffraction. The smoothness of the fracture face may well be considered as an illustration of the Reynolds–Sharp fracture mechanism in operation.

Possibly the first SEM images of fracture faces in high-modulus carbon fibres were those reported by Jones and Johnson [15], who also demonstrated evidence for buckling in the compressive region during bending in a loop test. Buckling

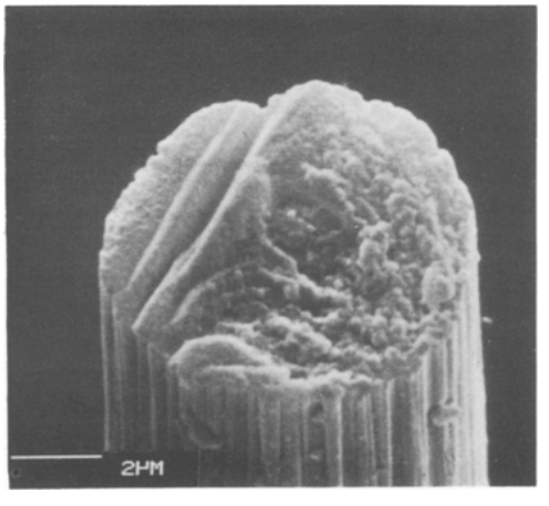

Figure 12 Fracture face of HM-S Grafil after flexural failure.

failure was considered to take place before ultimate failure from the region under tension. We have considerable experience of this type of failure in Kevlar-type fibres under flexural deformation [16]. Despite very careful observation of all fibres during knot closure in the SEM, and despite careful study of all the micrographs recorded before fibre failure, no evidence of buckling was noted in the carbon fibres which were the subject of this investigation.

Ewins and Potter [17] have suggested that a Reynolds–Sharp type mechanism, common to both tension and compression regions, is responsible for the initiation of failure in fibres fractured within a composite during longitudinal compression. Simultaneous on tension and compression regions may well be the reason why buckling or not there is any internal buckling not noticeable in SEM is a matter for further study.

5. Conclusions

It appears that the random structure of a circular cross-section Type I PAN-based carbon fibre leads to more flexibility and less brittleness than is the case with the more sheet-like structures of the high modulus mesophase-pitch-based fibres.

Essentially the same mechanism, that of Reynolds and Sharp, operates in both tensile failure and flexural failure.

A thorough examination of fibre deformation in a knot, particularly the surface strain, is needed before any convincing estimate of intrinsic tensile strength can be made.

*Lc, crystallite size in *c* direction; La, crystallite size in *a* direction.

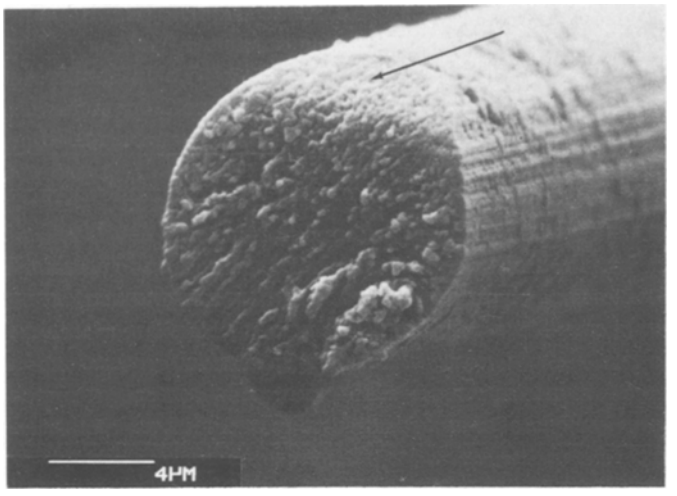

Figure 13 Fracture face of Thornel P after flexural failure.

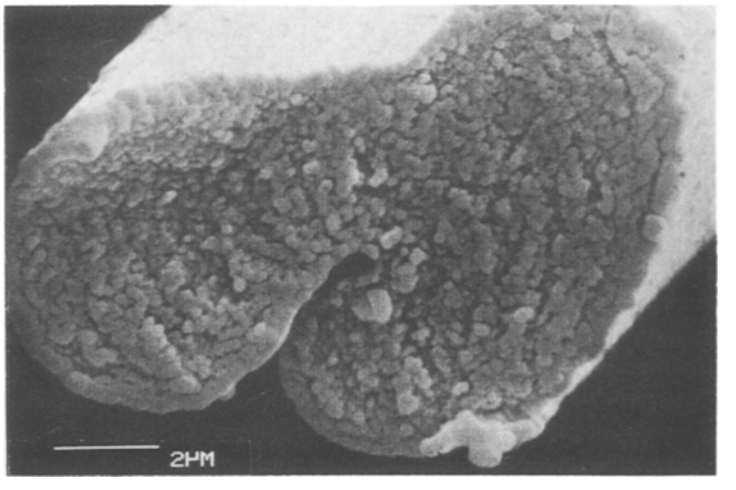

Figure 14 Fracture face of Celion GY-70 after flexural failure.

Acknowledgements

The authors are most grateful to Mr T. Buckley for his assistance with the SEM investigations. Mr Buckley also constructed the stage extensometer.

References

1. R. MORETON, *Fibre Sci. Technol.* **1** (1969) 273.
2. S. CHWASTIAK, J. B. BARR and R. DIDCHENKO, *Carbon* **17** (1979) 49.
3. J. W. JOHNSON, *Appl. Polymer Symp.* **9** (1969) 229.
4. J. W. JOHNSON and D. J. THORNE, *Carbon* **7** (1969) 659.
5. J. V. SHARP and S. G. BURNAY, "Carbon Fibres: Their Composites and Applications" (Plastics Institute, London, 1971) p. 68.
6. W. N. REYNOLDS, *Chem. Phys. Carbon* **11** (1973) 1.
7. S. C. BENNETT, D. J. JOHNSON and W. JOHNSON, *J. Mater. Sci.* **18** (1983) 3337.
8. J. B. JONES, J. B. BARR and R. E. SMITH, *ibid.* **15** (1980) 2455.
9. C. B. BEETZ, JR. *Fibre Sci. Technol.* **16** (1982) 45.
10. *Idem, ibid.* **16** (1982) 81.
11. D. J. THORNE, *Nature* **248** (1974) 754.
12. D. SINCLAIR, *J. Appl. Phys.* **21** (1950) 380.
13. ASTM Standard D2256-80.
14. D. J. JOHNSON, *Chem. and Ind.* 18 Sept. (1982) 692.
15. W. R. JONES and J. W. JOHNSON, *Carbon* **9** (1971) 645.
16. M. G. DOBB, D. J. JOHNSON and B. P. SAVILLE, *Polymer* **22** (1981) 960.
17. P. D. EWINS and R. T. POTTER, *Phil. Trans. Roy. Soc. Lond.* **A294** (1980) 507.

Received 5 October
and accepted 3 November 1983